Jet matching and subtraction methods for associated squark-gluino production

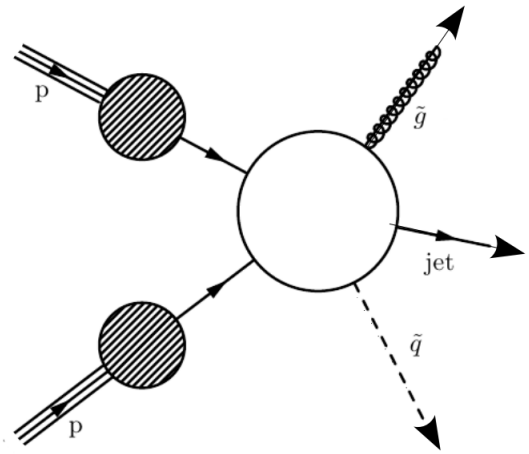

Bachelor Thesis in Physics
submitted by

Jennifer Kieselmann

born in Pforzheim (Germany)

WS 2011/2012

This Bachelor Thesis has been carried out by Jennifer Kieselmann at the
Institute for Theoretical Physics in Heidelberg
under the supervision of
Prof. Dr. Tilman Plehn

Abstract

In hadron-hadron collisions, e. g. at the Large Hadron Collider (LHC) at CERN in Geneva, one of the most promising signatures for physics beyond the Standard Model is jets plus missing transverse energy. In supersymmetric theories the most abundant production channels leading to jets plus a very large amount of missing transverse energy are pairs of heavy coloured particles: squarks and gluinos. To exclude or discover supersymmetric particles, it is essential to predict accurate theoretical cross sections for squark and gluino production and to study the shapes of kinematic distributions.

In this thesis, different subtraction methods for on-shell divergences in supersymmetric processes with the Monte Carlo generators MadGraph/MadEvent [5] and Pythia [34] are studied. Additionally, multijet matching and a comparison of jet matching to a full NLO calculation is performed using MadGolem for the NLO. The kinematic distributions for all subtraction methods agree well. The numerical subtraction that is implemented in MadGraph/MadEvent shows a slight dependence on the width. The NLO calculation is found to have a softer p_T spectrum as compared to MLM-jet matching. A comparison of diagram removal and analytical on-shell subtraction at the full NLO yields a softer p_T spectrum for the diagram removal.

Abstract (in deutscher Übersetzung)

Eine vielversprechende Signatur in Kollisionen von Hadronen, wie sie z.B. am LHC am CERN in Genf erzeugt werden, ist "Jets plus fehlende transverse Energie". In supersymmetrischen Theorien werden mit dieser Signatur hauptsächlich Paare von schweren, farbgeladenen Teilchen erzeugt, sogenannten Squarks und Gluinos. Um die Existenz supersymmetrischer Teilchen auszuschließen oder zu bestätigen, sind möglichst genaue Vorhersagen für die Größe von Wirkungsquerschnitten oder den Verlauf verschiedener kinematischer Verteilungen entscheidend.

In der vorliegenden Arbeit werden verschiedene Methoden untersucht, um On-Shell-Divergenzen in supersymmetrischen Prozessen zu beheben. Dafür werden verschiedene kinematische Verteilungen mit Hilfe der Monte-Carlo-Generatoren Pythia [34] und MadGraph/MadEvent [5] analysiert. Außerdem werden Prozesse mit unterschiedlicher Jet-Multiplizität verglichen und ein Vergleich zur nächsthöheren Ordnung (NLO) mit Hilfe von MadGolem gezogen. In allen Methoden ist der Verlauf kinematischer Verteilungen übereinstimmend. Für die numerische Methode in MadGraph/MadEvent wird eine Abhängigkeit von der Zerfallsbreite festgestellt. Jet-Matching weist, verglichen zu Simulationen in der nächsthöheren Ordnung, ein leicht härteres Spektrum für den transversalen Impuls auf. Ein Vergleich zwischen einer analytischen On-Shell-Subtraktion und dem expliziten Entfernen von potenziell resonanten Diagrammen zeigt, dass in letzterem Fall signifikante Beiträge zu größeren transversen Impulsen im Spektrum vernachlässigt werden.

Contents

1 Motivation and outline

The Standard Model of particle physics (SM) is a theory describing the electromagnetic, weak and strong interactions really successfully. It has been able to predict the results of various experiments and agrees perfectly with almost all current experimental data.

Nevertheless, there are several theoretical problems and open questions [25, 31]. The SM describes only three of the four known fundamental forces. It does not include a theory of gravity. In addition, no candidate for dark matter is provided by the SM: According to cosmological measurements [27] dark matter makes up about one quarter of the whole matter content of the universe, whereas visible matter only contributes 5% [18, 20].

Furthermore, the SM predicts the existence of the Higgs boson. The Higgs boson is a consequence of the Higgs mechanism, which is supposed to give masses to the gauge bosons W and Z of the SM as well as to the fermions through electroweak symmetry breaking. But, as of this writing, this particle has not yet been discovered. Neither can the SM explain the evident asymmetry between baryonic and antibaryonic matter; without the asymmetry, the universe would not contain any matter but photons only. Other problems are the hierarchy or fine-tuning problem as well as gauge coupling unification [24].

Considering all these aspects it is clear that even though it is an extremely successful effective theory, the SM has to be extended to some underlying deeper theory that can provide solutions to these open questions and problems. Various new models are based on Supersymmetry [24], such as the Minimal Supersymmetric extension of the Standard Model (MSSM).

Since signs of new physics beyond the SM are expected at higher energy scales, there are many experiments looking for such signals. For instance, the Large Hadron Collider (LHC), a proton-proton collider at CERN in Geneva, has been running and producing a large amount of data since 2009. It is constructed to find the Higgs boson as well as to discover new physics beyond the SM. To interpret the measurements correctly, it is crucial to make precise predictions for different theories beforehand. This is done with the help of Monte Carlo simulations.

In theory and in a realistic simulation of particle collisions several problems exist. There are for example divergences (ultraviolet, infrared and on-shell) that do not appear in nature and thus have to be removed from the theory. In this work, different methods used in Monte Carlo simulations for the purpose of removing on-shell divergences are studied.

The thesis is structured as follows: In chapter 2, the basic theoretical concepts that underlie this work are reviewed. A brief introduction into phenomenological and technical aspects is given. In chapter 3, different theoretically motivated concepts and methods for removing on-shell divergences are analysed with the help of the Monte-Carlo generators MadGraph/MadEvent [5] and Pythia [34]. The analytical on-shell subtraction is studied in more detail in chapter 4. Different jet multiplicities are compared in chapter 5. I conclude in chapter 6.

2 Theoretical background

This chapter gives a brief introduction into the theoretical background of this work. In section 2.1, the basic ideas and concepts of Supersymmetry and the MSSM are sketched. The relevance of squark-gluino production is reviewed. In section 2.2, essential technical concepts are described: jets in QCD, the idea of jet matching and different methods that are used in this work to remove on-shell divergences.

2.1 Phenomenological aspects

2.1.1 Supersymmetry and the MSSM

Many of the theories desribing new physics that have been proposed so far are based on Supersymmetry (SUSY) [24]. This new symmetry provides solutions to several problems in the SM. Among others, SUSY can solve the fine-tuning problem and the deeply connected hierarchy problem.[1] It leads to the desired unification of the electromagnetic, weak and strong interactions and provides a candidate for the dark matter particle. In this model, the dark matter particle is a WIMP (Weakly Interacting Massive Particle).

Supersymmetry is a symmetry that relates bosonic to fermionic fields. There are various models that make use of this general concept. This work is based on a Minimal Supersymmetric extension of the Standard Model, the MSSM. It features a minimal set of fields and couplings.

For each field in the SM there is a supersymmetric partner that has the same quantum numbers except for spin. The particle spectrum can be found in table 2.1. The superpartners of the quarks are provided with indices for left- and right-handed particles. As they are bosons, these indices do not correspond to chirality, but indicate that they are the partners of the left- and right-handed quarks, respectively. Their left- and right-handed nature is reflected in their gauge couplings (e. g. the left-handed squarks couple to the W-boson, whereas the right-handed ones do not). More details can be found in [24].

[1] In the SM, there is no explanation for the huge range of forces between the weak force and gravity. Neither can it explain why the Higgs particle is light if there are large quadratic quantum corrections to its mass. This would involve an extreme fine-tuning. SUSY can provide a solution to this problem because the supersymmetric partners would precisely cancel the leading quantum corrections.

SM content			SUSY partners		
field		spin	field		spin
gauge field	$W^{\pm}, Z, \gamma, g$	1	gaugino	$\widetilde{W}^{\pm}, \widetilde{Z}, \widetilde{\gamma}, \widetilde{g}$	$\frac{1}{2}$
Higgs	H	0	Higgsino	$\widetilde{H}$	$\frac{1}{2}$
quark	$q_{L/R}$	$\frac{1}{2}$	squark	$\widetilde{q}_{L/R}$	0
lepton	$l_{L/R}$	$\frac{1}{2}$	slepton	$\widetilde{l}_{L/R}$	0

Table 2.1: This table provides an overview of all fields in the MSSM. For each SM field, there is a supersymmetric partner that has the same quantum numbers except for spin.

In the MSSM, a so-called R-parity conservation is imposed. As a consequence, SUSY particles can only be produced pairwise: R is defined as R$= (-1)^{2S+3B+L}$ with S being the spin, B the baryon number and L the lepton number. For SUSY particles therefore holds R$= -1$, whereas for SM particles R$= 1$. R-parity is a multiplicitive quantity. If R-parity is conserved, then SUSY particles can only appear in pairs.

The MSSM involves many free parameters that have to be fixed. In this work, I use a modified SPS1a-benchmark point (SPS1a_{1000}) and, for reasons of comparison to an inverted gluino-squark mass hierarchy, the benchmark point SPS8 [7]. Current bounds on the masses of supersymmetric particles derived from the so far negative searches at colliders [2, 6, 15] imply that the gluino mass should be larger than the prediction in the SPS1a benchmark point. For this reason, I use a modified SPS1a-benchmark point, in which the gluino mass is set to a larger value. All parameters are listed in table 2.2.

2.1.2 Relevance of squark-gluino production

The search for SUSY is one of the main purposes the LHC has been constructed for. In hadron-hadron collisions coloured particles are created. For this reason squarks and gluinos, the coloured particles in the MSSM, would be produced most abundantly. As a consequence of R-parity conservation, SUSY particles only appear in pairs. The most interesting processes thus are the production of a squark pair, a gluino pair or the associated production of a squark and a gluino [2, 6, 8, 15, 30].

To set exclusion limits on the masses of SUSY particles or, in case of discovery, determine their masses and properties, it is crucial to predict precise theoretical cross sections for squark and gluino production. This search is done for the signature jets plus missing transverse energy: Since gluinos and squarks are coloured particles, they radiate off gluons and lead to a cascade of subsequent coloured particles. In the detectors, jets plus an additional amount of missing transverse energy are observed due to the lightest supersymmetric particle (LSP). The LSP is colour-neutral, stable as a consequence of R-parity and escapes the detectors unobserved.

The main difference to SM background processes is that a large amount of missing transverse energy is expected [30]. In order to enhance the signal, the parameter 'missing

specification	parameter	value	comment
SPS1a$_{1000}$	$m_{\tilde{u}_L}$	561 GeV	
	$m_{\tilde{u}_R}$	549 GeV	
	$m_{\tilde{g}}$	1000 GeV	due to current bounds from SUSY searches
SPS8	$m_{\tilde{u}_L}$	1113 GeV	
	$m_{\tilde{u}_R}$	1077 GeV	
	$m_{\tilde{g}}$	839 GeV	
run parameters	$\sqrt{s}$	7 TeV	center-of-mass energy
	nevents	500000	number of requested events
	μ_F, μ_R	$\frac{1}{2} \cdot (m_{\tilde{u}_L} + m_{\tilde{g}})$	factorisation and renormalisation scales
	PDFs	CTEQ6L1	parton distribution function
	ickkw	1	MLM-type matching
	ktscheme	2	PYTHIA p_T ordered
	bwcutoff	15	for the definition of on-shell
	xqcut	60 GeV	minimum k_T-jet-measure between partons
	$\|\eta\|$	≤ 5	cut on pseudo-rapidity for quarks
	R_{ij}	≥ 0.4	angular distance between two jets

Table 2.2: Important parameters used in this work. The first two parts list the masses coming from two different Snowmass benchmark scenarios, a modified version of SPS1a and SPS8. The widths for these particles are set to zero. All other parameters from the SPS benchmark points, which are irrelevant for this study, can be found in [7]. The third part lists the important parameters that are used in MADGRAPH/MADEVENT and PYTHIA in this work.

transverse energy' has to be restricted from below.

The leading order Feynman diagrams for squark-gluino production are shown in figure 2.1. All Feynman diagrams in this thesis have been created using the LaTeX tool FeynMF [29].

2.2 Technical aspects

2.2.1 QCD and jets

At the LHC, protons are accelerated and brought to collisions. Protons are non-fundamental particles. They are hadrons that are built up of smaller, elementary particles: quarks and gluons. The interactions of quarks and gluons are described by the theory of Quantum Chromodynamics (QCD), a non-abelian gauge theory of the strong force. To extract new physics from data a deep understanding of the usual SM physics, i. e. in this case especially QCD processes, is important.

To analyse the data, usually a separation in background and signal is done. Background is the simulation of all particles and interactions that are known and unterstood so far.

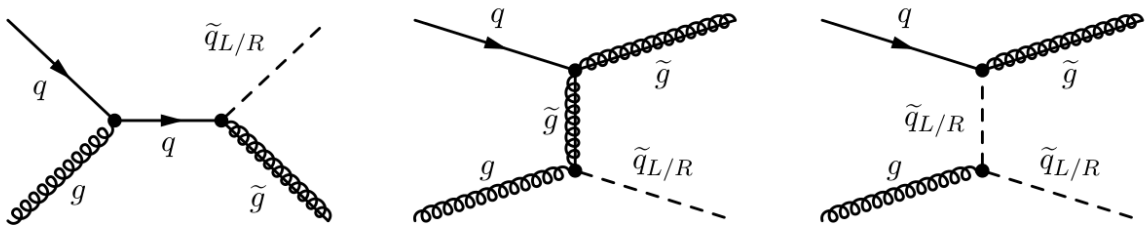

Figure 2.1: Leading order Feynman diagrams for associated squark-gluino production through proton-proton collisions: $qg \to \tilde{g}\tilde{u}_L$

Signal refers to new particles to be found or understood. This includes simulations of new physics based on different theories as well as the experimental data. Simulating the background properly is a difficult task because coloured particles radiate off gluons and produce a lot of other particles via QCD radiation and decays. Since possible signs of new physics are strongly influenced by this radiation or even hidden it is crucial to predict their features properly. If new physics in form of new strongly interacting particles exists at the TeV scale, typically large amounts of energy and missing transverse energy in the detectors as well as several hard jets from the decay of these heavy particles are observed [3, 30, 31].

Jets

Due to colour confinement in QCD, all freely existing particles have to be colour-neutral. Quarks and gluons as coloured particles are combined to colour-neutral hadrons through a fragmentation and hadronisation process. For this reason, no free quarks are observed in the detectors, but tracks of bunches of particles. These narrow cones of particle tracks generated by hadronisation are called jets. It is not trivial to identify different jets, as they are usually boosted together, i. e. they are not really separated and overlap.

There are various jet algorithms and jet definitions that describe and allow to reconstruct those jets in order to extract the original process. Here, a k_T-jet algorithm [12] is used. In order to exemplify the procedure, this jet algorithm is described in more detail. The procedure for this algorithm is common to all recombination algorithms.

Example: k_T-jet algorithm The basic lines of the procedure can be summarised as follows:

1. A list of preclusters is singled out, i. e. lists of 4-momentum-vectors ordered by decreasing 4-momentum.

2. For each precluster the value of $d^i = (k_T^i)^2$

   and for each pair of preclusters $d^{ij} = \min\left((k_T^i)^2, (k_T^j)^2\right) \cdot \frac{(R^{ij})^2}{D}$ is calculated where

   - k_T is the transverse momentum
   - R^{ij} is the angular distance, $R = \sqrt{(\Delta\phi)^2 + (\Delta y)^2}$
   - $\Delta\phi$ is the difference of the polar angles ϕ^i and ϕ^j
   - Δy is the difference of the rapidities y^i and y^j
   - D is an algorithm-specific value ($D \approx 1$)

3. The minimal value $d_{\min}$ of all d's from preclusters is determined:

$$d_{\min} = \min\left(\{d^i, d^{ij}\}\right).$$

   If

   - $d_{\min}$ is one of the d^{ij}'s, a combined precluster is built out of the two preclusters by adding their 4-momenta. The procedure restarts at point 2.
   - $d_{\min}$ is one of the d^i's, this precluster is defined as jet. If there are any objects left on the list of preclusters, the procedure starts again at point 2, excluding this jet. Otherwise it ends here.

2.2.2 Monte Carlo simulation

According to the factorisation theorem in QCD (see e. g. [19, 31]) one can factorise the cross sections for hadronic collisions at high energies into a so-called 'hard scattering' process, which is at parton level, and parton distribution functions:

$$\sigma_{tot} = \int_0^1 dx_1 \int_0^1 dx_2 \sum_{jk} f_j(x_1) f_k(x_2) \sigma_{jk}(x_1 x_2 s).$$

The f_i are parton distribution functions (PDFs) describing the probability to find a parton, i. e. a quark or a gluon, inside the hadron (here proton) for a specific x_i; x_i is the momentum fraction of one parton inside the proton and s is the center-of-mass energy of the two colliding protons.

The cross section at parton level can be calculated perturbatively in QCD. The parton distribution functions take into account the non-perturbative part of the process. There, an order-by-order calculation of the matrix elements is not valid. To describe this non-perturbative part properly there are formalisms available like e. g. the Parton Shower (PS) formalism [31]. Parton showers can describe processes at arbitrary high orders in α_s, but only in the leading logarithmic approximation of transverse momentum. It

describes the evolution of quarks and gluons by taking into account probabilities for splitting into further partons.

In order to simulate data at colliders and detect possible deviations from the SM, Monte Carlo simulations are performed. There are various Monte Carlo simulators, adequate for different purposes. In this work, I use a combination of MadGraph/MadEvent [5] and Pythia [34].

The procedure is as follows: MadGraph creates the matrix elements for a specified process. MadEvent generates events on a statistical basis at parton level and the cross sections are computed. Thanks to an interface between MadGraph/MadEvent and Pythia, the generated events can be used in Pythia, where the events at parton level are showered according to a specific shower scheme. If desired, Pythia decays the final particles and simulates the subsequent hadronisation process.

By means of this strategy, one can quite realistically simulate the experimental signature of collisions at hadron colliders like the LHC. For a comparison with the full NLO the yet-to-be-published MadGolem, which is an expansion of MadGraph/MadEvent to NLO, is used.

2.2.3 Jet matching

The Parton Shower formalism is by construction only valid in the limit of soft (low energy) and collinear (small angles with respect to the beam) gluon radiation. For hard and widely separated gluon radiation jets this description breaks down and perturbative matrix element calculations have to be used. The Matrix Element approach, i. e. an order-by-order calculation in the strong coupling constant α_s, however, diverges in the limit of soft and collinear emission. In this regime, the strong coupling constant α_s takes values of order $\mathcal{O}(1)$ and therefore a perturbative approach is no longer valid.

As both regimes coexist, it is essential for a complete description of the events to consider the full matrix elements for the underlying hard processes as well as the parton showers that describe the evolution of the hard partons into jets of hadrons. The exact limits in phase space between the two are not clearly defined. Thus, for each event it has to be decided which of the two descriptions shall be applied.

Different methods solving this problem are so-called matching schemes. Examples are the CKKM scheme [14], the Lönnblad scheme [21] or the MLM scheme [22, 23]. The crucial aim of all these schemes is to avoid double counting of events as well as regions where none of the two descriptions applies. An important condition for all matching schemes is to require smooth transitions between the regions that are described by parton showers, i. e. for values smaller than Q_{match}, and the regions described by the Matrix Element approach, i. e. values larger than Q_{match}, where Q_{match} is the scale separating those two. In addition, the distributions should not depend on the matching scale, so they have to be stable under its variation.

In my thesis, I use specific version based on the MLM scheme, the k_T-jet MLM scheme [3] implemented in MadGraph/MadEvent. In the following part, I will briefly explain the basic steps in this procedure of jet matching.

k_T-jet MLM scheme

In the k_T-jet MLM scheme one first generates all events with different parton multiplicities. The final-state partons are then clustered according to a k_T-jet algorithm as explained in section 2.2.1. The k_T-value is limited to be above some cutoff scale:

$$k_T > Q_{\text{cut}}^{\text{ME}}.$$

The event at parton level is then sent to Pythia for showering. Before hadronisation and the decay of the particles will take place, the partons are again clustered into jets using the k_T-jet algorithm. The momentum is restricted to some lower limit

$$Q_{\text{match}} > Q_{\text{cut}}^{\text{ME}}.$$

These jets are then compared to the original partons from the event before showering. A jet is matched to a closest parton if the jet measure fulfills

$$k_T(\text{parton,jet}) < Q_{\text{match}}.$$

Exceptions are the highest-multiplicity samples, i. e. samples with the largest number of partons, where smaller transverse momenta are allowed:

$$k_T < Q_{\text{softest}}^{\text{ME}}.$$

Only events where all jets are matched to partons are kept. If two partons are for example too close to create two distinct jets, the event is rejected. This procedure prevents double counting and is infrafred and collinear safe. Furthermore, the MLM scheme ensures that parton shower radiation is limited to its appropriate (soft and collinear) regions of phase space.

In the following parts of this thesis, I will use the terms 'final state partons' and 'jets' synonymously, keeping in mind how they are related.

2.2.4 Double counting and subtraction schemes

A theoretical problem in the simulation of these events is double counting[2] due to resonant diagrams [3].

[2]Double counting is not specific to supersymmetric processes. It can also appear in usual SM processes when a final state can be reached through different cascades of particles.

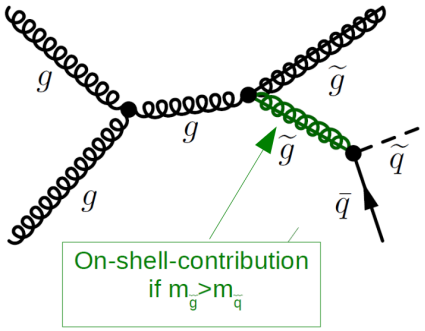

Figure 2.2: **Feynman diagram for the production of a squark and a gluino with an additional quark jet:** $gg \to \tilde{g}\tilde{g}^{(*)} \to \tilde{g}\tilde{q}\bar{q}$**.** The quark jet and the squark are produced via a gluino. Depending on the mass hierarchy, this gluino propagator can be on-shell, leading to a resonance. However, if the gluino is on-shell, this particular process is already taken into account in the production of two gluinos with the subsequent decay of the gluino into a squark and a quark.

In order to illustrate how double counting arises, associated squark-gluino production is considered. This process is of special interest in searches for SUSY, see section 2.1.2. A subprocess in squark-gluino production through proton-proton collisions is:

$$gg \to \tilde{g}\tilde{q} \text{ (at order } \alpha_s^2).$$

At NLO there are processes like

$$gg \to \tilde{g}\tilde{g} \to \tilde{g}\tilde{q}\bar{q} \text{ (at order } \alpha_s^3).$$

A Feynman diagram for this NLO process is depicted in figure 2.2. If the mass hierarchy is given as $m_{\tilde{g}} > m_{\tilde{q}}$, there is an on-shell contribution to the matrix element when the momentum flow reaches the gluino mass. This on-shell contribution is already included in the Born process $gg \to \tilde{g}\tilde{g}$ with the subsequent decay $\tilde{g} \to \tilde{q}\bar{q}$ for example through the Parton Shower formalism. Thus, one has to subtract it properly to avoid double counting if one wants to add the associated squark-gluino and the gluino pair production rates not only at LO, but also at NLO. For this purpose there are different kinds of subtraction schemes.

In chapter 3, the characteristics of different subtraction methods are compared by analysing different distributions. In this section, the theoretical ideas are considered.

Method A. Only radiation of gluons allowed

A method to avoid double counting and remove on-shell divergences is to consider additional gluon jets only since in this case there are no resonant diagrams left. Processes involving gluon jets which are radiated off the final states are dominant as compared

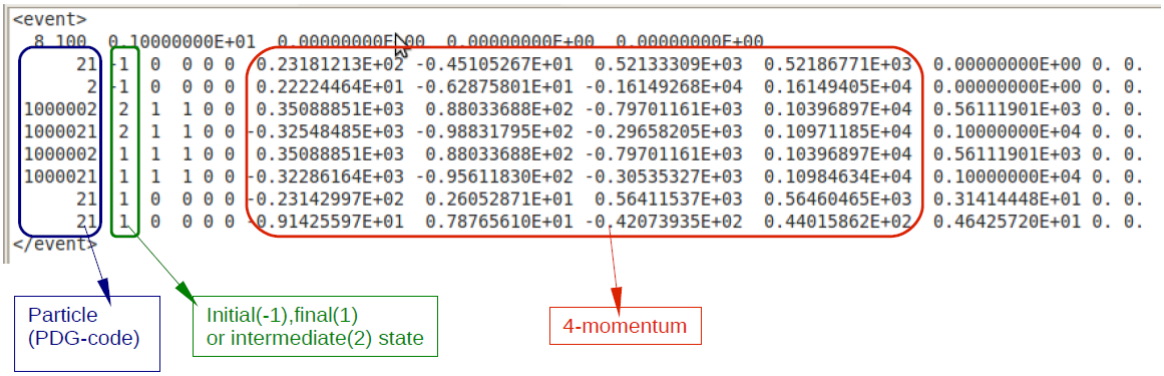

Figure 2.3: **Example for an event as it is produced by MadEvent.** For each event there is a PDG code which assigns the particle, a number marking the particle as initial, final or intermediate state, the values of the 4-momenta, spins etc.

to others – in the present example additional quark jets, in which heavy intermediate particles (squarks and/or gluinos) are involved. Such contributions are phase-space suppressed by inverse powers of the mass of these intermediate states. For this reason, considering only gluon jets is a reasonable assumption. Although it is a very simple method and violates gauge invariance, it is a numerically valid approximation which can be seen also in chapter 3.

Method B. Explicit diagram removal

Another possibility is to explicitly remove the resonant diagrams [3, 30], i. e. all diagrams involving a resonant gluino (or, in case of an inverted squark-gluino mass hierarchy, a resonant squark). This procedure also violates gauge invariance, but it is a reasonable approximation for small widths of the resonant state, i. e. for $\Gamma/m \ll 1$. The interference terms are neglected in this scheme. They are usually proportional to Γ/m, so one can neglect them for small widths. The disadvantage of this method is that also off-shell contributions away from the pole are removed. These contributions might contribute significantly to the total rate and are in this scheme neglected.

Method C. A numerical subtraction in MadGraph/MadEvent

MadGraph/MadEvent provides a method which is a hybrid between a gauge-invariant subtraction and the diagram removal [3]. During the procedure of generating the events a file is created that lists all the events that are produced. This includes the values of 4-momentum vectors, the spin configuration, the identities of the particles and their status. An example for an event can be seen in figure 2.3. Before showering, one can

use the EXCRES parameter (excluded resonance) implemented in MADGRAPH/MADEVENT and PYTHIA. To mark a particle as excluded resonance one just has to add the line EXCRES=N_{pdg} to the configuration file pythia-card for each particle one wants to exclude as intermediate resonant particle. N_{pdg} is the code corresponding to the Particle Data Group for that particle [11].

Events containing excluded resonant propagators are rejected before they are passed to PYTHIA. The information about a particle being resonant is listed in the event file. There each particle is flagged as initial (-1), final (1) or intermediate resonant (2) state (marked in green in figure 2.3). The 2 appears if the particle is an intermediate on-shell particle. On-shell is defined by

$$|M - m_p| \leq \Gamma_p \cdot \text{bwcutoff}, \tag{2.1}$$

where M is given by the momentum, m_p is the physical mass, Γ_p the width of the particle and bwcutoff can be set in the run-card. This is a configuration file in which all parameters for the event generation, e. g. the CMS energy, statistics and various cuts on kinematic variables can be set. The default value for bwcutoff is 15 and used in this work.

In this scheme, the width is not necessarily the physical width of the particle. It is only used as some cutoff parameter in phase space. Since the definition of on-shell depends on this value the cross section might also depend on the variation of this width. This possible dependence is further studied in section 3.3.

In summary, using the EXCRES option resembles a numerical cut in phase space: in contrast to diagram removal where the whole diagram is removed, regions around the singularities depending on the parameters in equation 2.1 are cut off.

Method D. An analytical subtraction: Prospino scheme

In order to handle double counting in the PROSPINO scheme [8, 9], first a separation of the process in off-shell and on-shell contributions is done. To see this explicitly, the example process from above ($gg \to \tilde{g}\tilde{g}^{(*)} \to \tilde{g}\tilde{q}\bar{q}$) is considered. The notations $\tilde{g}^*$ and $\tilde{g}$ stand for off-shell and on-shell gluinos, respectively. For computational convenience, a remapping of the phase space is done. The matrix element is split into a resonant and a regular part:

$$\begin{aligned} |\mathcal{M}|^2 = |\mathcal{M}^{\text{res}} + \mathcal{M}^{\text{reg}}|^2 = |\mathcal{M}^{\text{res}}|^2 + 2 \cdot |\mathcal{M}^{\text{res}} \cdot \mathcal{M}^{\text{reg}*}| + |\mathcal{M}^{\text{reg}}|^2 \\ \text{with } \mathcal{M}^{\text{res}} = \mathcal{M}_{gg\to\tilde{g}\tilde{g}\to\tilde{g}\tilde{q}\bar{q}} \text{ and } \mathcal{M}^{\text{reg}} = \mathcal{M}_{gg\to\tilde{g}\tilde{g}^*\to\tilde{g}\tilde{q}\bar{q}}. \end{aligned} \tag{2.2}$$

To regularise the potentially divergent propagator, a finite width Γ_{os} for the possible on-shell particles is introduced as a mathematical cutoff. The plain propagator is then

transformed into a Breit-Wigner (BW) propagator:

$$\frac{1}{p^2 - m_{\text{os}}^2} \to \frac{1}{p^2 - m_{\text{os}}^2 + im\Gamma_{\text{os}}} \quad (\text{with } \Gamma_{\text{os}} = \Gamma_{\tilde{g}}) \tag{2.3}$$

After integration over phase space the resonant part gives the same contribution as the one from the Born process with the subsequent decay:

$$gg \to \tilde{g}\tilde{g} \quad \times \quad \tilde{g} \to \tilde{q}\bar{q}.$$

So the on-shell part in the present example is for each phase space point subtracted as follows:

$$\sigma = \int_{2+1jet} (d\sigma^{reg} + d\sigma^{res}(\Gamma_{\tilde{g}}) - d\sigma^{CT}(\Gamma_{\tilde{g}})) \tag{2.4}$$

$$\text{with } d\sigma_{LO}^{CT}(\Gamma_{\tilde{g}}) = \sigma_{gg\to\tilde{g}\tilde{g}} \cdot \frac{m_{\tilde{g}}\Gamma_{\tilde{g}}/\pi}{(p^2 - m_{\tilde{g}}^2)^2 + m_{\tilde{g}}^2\Gamma_{\tilde{g}}^2} \cdot BR(\tilde{g} \to \tilde{q}\bar{q})$$

In terms of diagrams, this corresponds to the following:

$d\sigma$ 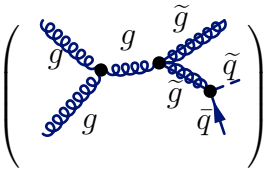 $-\, d\sigma$ 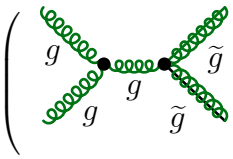 $\times$ 'BW' $\times$ BR 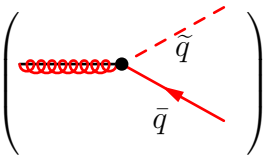

After the subtraction the width is set back to zero, since it serves only as mathematical cutoff. In the small-width limit, the Breit-Wigner turns into a δ-distribution:

$$\lim_{\Gamma_{\tilde{g}} \ll m_{\tilde{g}}} \frac{1}{(p^2 - m_{\tilde{g}}^2)^2 + m_{\tilde{g}}^2\Gamma_{\tilde{g}}^2} \to \frac{\pi}{m_{\tilde{g}}\Gamma_{\tilde{g}}} \cdot \delta(p^2 - m_{\tilde{g}}^2). \tag{2.5}$$

The Breit-Wigner term in equation 2.4 is then replaced by a δ-distribution, giving the on-shell condition.

This procedure is gauge-invariant, preserves the spin correlation and furthermore, the dependence on the regulator Γ_{os} cancels in the end. It is not yet implemented in the LO in MadGraph/MadEvent. Instead, it is part of the automated full NLO package MadGolem. For finite width the Prospino scheme is implemented in MC@NLO [17].

3 Subtraction methods

In this chapter I use the methods to handle on-shell divergences in MadGraph/MadEvent interfaced with Pythia and compare their behaviour for distributions of the differential cross section depending on the transverse momentum and the rapidity of the heavy final states.

3.1 Kinematics and parameters

Since collisions of two hadrons that consist of partons are considered, the kinematics is not as simple as e. g. in electron-positron scattering. The centre-of-mass frame (CMS) of the partons is not the same as the CMS of the hadrons, which is in this case the lab frame of the collision. For simplicity, the partonic CMS is assumed to be boosted along the beam axis (z-axis), i. e. all partons inside the proton have zero transverse momenta.

In order to have a useful description of the kinematics one needs to find boost-invariant variables. An adequate choice of variables is (p_T, y, ϕ). The transverse momentum p_T is not affected by a longitudinal boost. The rapidity y, defined as

$$y = \frac{1}{2} \cdot \frac{E + p_z}{E - p_z}, \tag{3.1}$$

where z is the longitudinal beam axis, is additive under Lorentz-boosts. Hence, the shape of $d\sigma/dy$ stays the same after a Lorentz boost with a constant velocity β. The azimuthal angle ϕ (angle around the beam axis) is also boost-invariant.

The parameters are set according to table 2.2 unless stated otherwise. Since the LHC is currently running at a centre-of-mass energy $\sqrt{s} = 7$ TeV, I use this value. To get enough statistics, the number of events randomly generated by MadEvent is set to 500000 using the MultiRun-feature of MadGraph/MadEvent. For the PDF of the partons inside the proton, I use CTEQ6L [33] with four active flavours. The factorisation and renormalisation scales μ_F^0 and μ_R^0 are set to the average mass of the heavy final states. For the matching procedure I use a MLM-type matching, implemented in MadGraph/MadEvent as described in section 2.2.3.

Several cuts on variables are applied. They are used to separate the hard matrix element part (hard jets) from the parton shower (soft and collinear jets). The minimum k_T-jet

measure between the partons is set to 60 GeV, as it is recommended in [3]. The pseudorapidity of the jets is restricted to $|\eta| \leq 5$. These variables can be further restricted in a detector simulation to reject more background processes and therefore enhance the signal as well as to simulate realistic detectors which for example can not cover the full range of pseudorapidity. This is not done here.

With the help of MadGraph the scattering process of two incoming protons is generated. The outgoing particles are a gluino and a squark, where for simplicity only the lightest squark is used, i. e. the superpartner $\tilde{u}_L$ of the left-handed up quark. A second process is added, which involves an additional hard jet: a gluon or an (anti-)quark, where without loss of generality only up quarks are considered. Other generations and down-type quarks are neglected. This will not change the qualitative results but only the total cross section, which is not important here. The jets can be final state radiated (FSR) or initial state radiated (ISR).

All distributions in this thesis are for events including (0+1) additional hard jets, i. e. the matching of leading order processes and leading order plus one additional hard jet, unless stated otherwise. MadEvent randomly generates events, which are then showered by Pythia. Both final states, the squark and the gluino, are set stable so they will not decay into lighter particles during the showering procedure. This is done in order to study the differences in the treatment of on-shell divergences; including the decay would not add new phenomenological features.

3.2 Gluon radiation versus diagram removal

The methods A (gluon radiation) and B (diagram removal), introduced in section 2.2.4, are compared. All distributions are obtained by a combination of MadAnalysis (see [4]) and Grace [32]. MadAnalysis is a simple analysis tool available as additional package in MadGraph/MadEvent with output in ASCII files.

3.2.1 Distribution in transverse momentum p_T

Assuming the z-axis to be the beam axis, the transverse momentum is given as

$$p_T = \sqrt{p_x^2 + p_y^2}. \tag{3.2}$$

The distributions are shown in figure 3.1. The dependence of the differential cross section on the transverse momentum is plotted for the two final state particles, the gluino and the squark. The distributions are for both methods normalised to their total cross section, respectively. For each diagram the green curve is created using method A, whereas the red one follows from B.

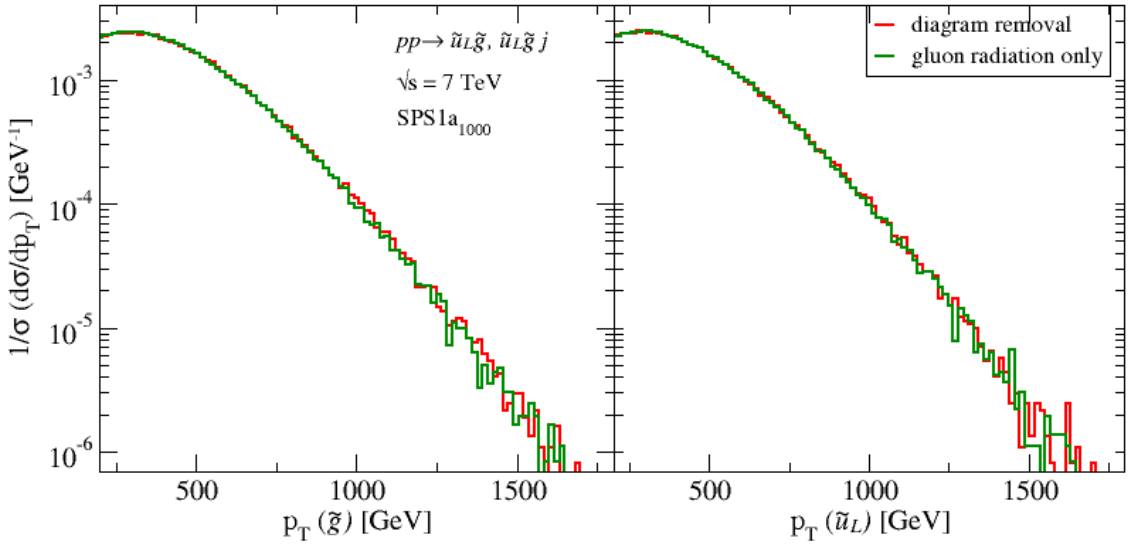

Figure 3.1: **The normalised differential cross section $\frac{d\sigma}{dp_T}$ for the two final states (gluino and squark).** The red lines correspond to diagram removal, the green ones to gluon radiation only. The red and green distributions look very similar. The values for the total cross sections are different in the two methods, but the interesting point is their kinematical distribution.

The distributions in general for both heavy final states are very similar. The distribution for the gluino is slightly harder, which means that it is shifted to larger values of p_T in comparison to the distribution for the squark. This makes sense because the gluino has a larger mass than the squark in SPS1a$_{1000}$, which I used here.[3]

The shapes of the distributions for method A and B do agree well. There is no significant difference. This agreement can be explained by the suppression in phase space: Diagrams with gluon jets radiated off the final state particles do not involve an intermediate heavy particle, whereas in contrast diagrams with quark jets radiated off the final states include an intermediate squark and/or a gluino. As the matrix elements and thus also the cross sections are proportional to powers of the inverse mass of the intermediate particles, diagrams with final state quark jets are suppressed. Hence, gluon jets are preferred produced and the main part of the population of the p_T spectrum comes from those events. Thus, the simplification of only allowing for gluon jets is reasonable.

Despite this, the total cross section values for both cases are different. It has been found that, as expected, for method A the cross section is smaller compared to method B. This can not be seen in the plots, as the distributions are normalised to their total cross sections, because the main focus here is on the shape of the distributions.

The difference between method A (gluon radiation) and method B (diagram removal)

[3]The difference is even more significant, if one compares in addition the distributions of the two heavy particle final states to the ones for the (massless) SM-particles, i. e. the extra jet.

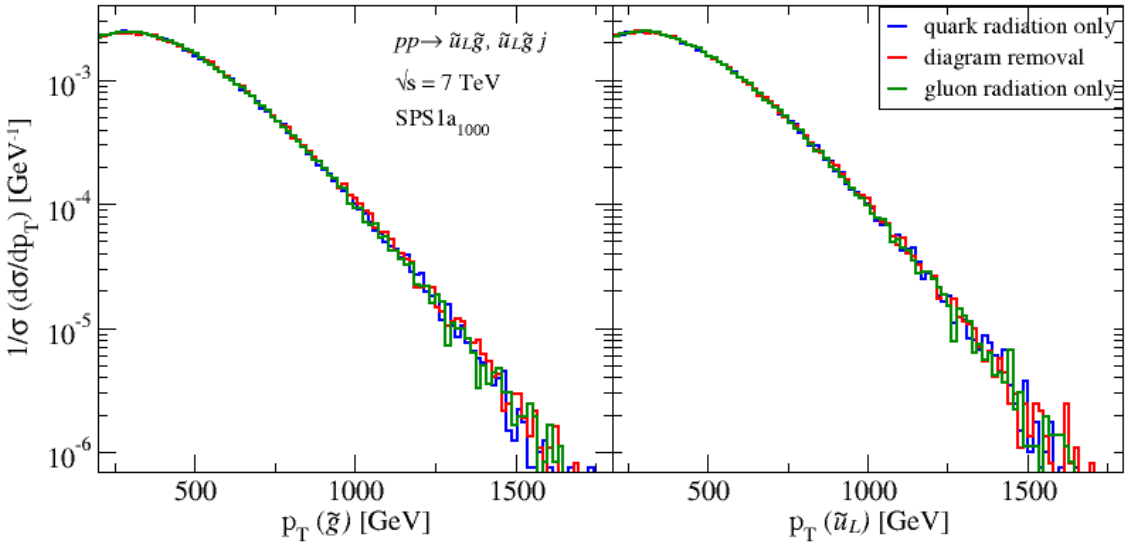

Figure 3.2: **The normalised differential cross section $\frac{d\sigma}{dp_T}$ for the two final states, including the distribution involving only quark jets for consistency check.** The green line corresponds to method A, the red line to method B. The blue line shows the distribution where only quark jets are involved, including diagram removal by hand for diagrams involving potentially on-shell gluinos. The shape is basically the same so consistency is confirmed.

is that in the first case, quark jets are neglected. To check for consistency, the distribution with only quark jets – removing the potentially resonant diagrams by hand – is additionally plotted in figure 3.2: Since the shape for gluon radiation is very similar to the one for diagram removal, the shape for quark radiation, excluding potentially resonant diagrams, is expected to be also very similar, provided that all distributions are normalised such that their integral yields 1. This expectation is confirmed as can be seen in figure 3.2.

The value for the cross section is now even smaller. This fact becomes clear by the same arguments as before: due to the masses of the intermediate particles, in this case squarks or gluinos, quark jets are suppressed in comparison to gluon jets.

3.2.2 Distribution in rapidity y

The rapidity y of a particle with energy E, mass m and momentum p is given by

$$\begin{aligned} y &= \frac{1}{2}\ln\frac{E+p_L}{E-p_L} = \frac{1}{2}\ln\frac{(E+p_L)^2}{m^2+p_T^2} = \ln\frac{E+p_L}{m_T} \\ &= \frac{1}{2}\ln\frac{1+\beta\cos\theta}{1-\beta\cos\theta} = \operatorname{artanh}(\beta\cos(\theta)). \end{aligned} \tag{3.3}$$

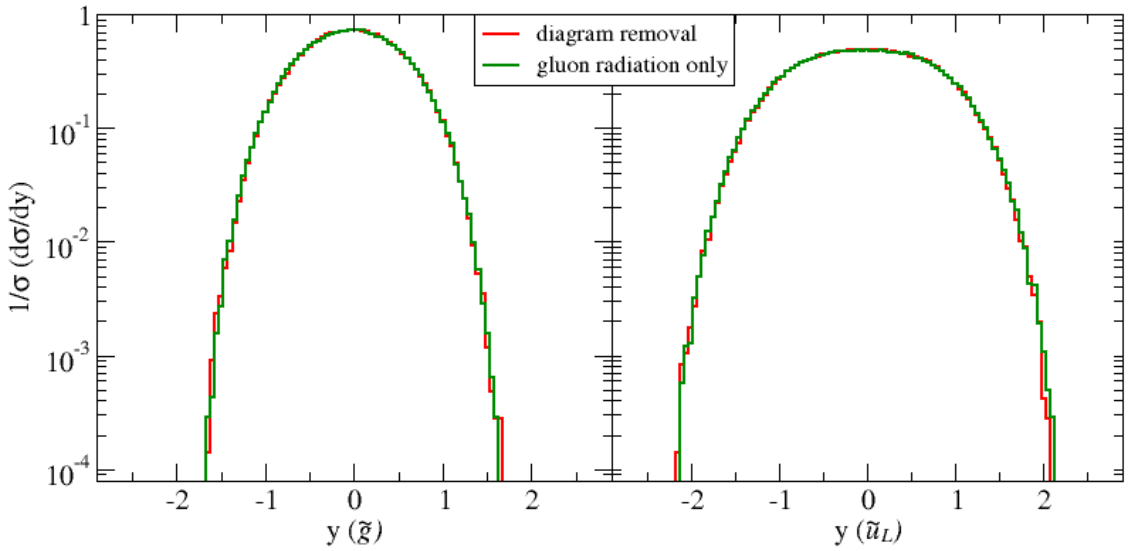

Figure 3.3: **The normalised differential cross section $\frac{d\sigma}{dy}$ depending on the rapidity y for each of the two final states.** The red curves correspond to method B, the green ones to method A. In both final states, the shapes of the distributions agree quite well.

Here p_L is the component of the momentum along the beam axis, θ is the polar angle and $\beta = p/E$ the velocity. In the limit of massless particles ($E \approx |\vec{p}|$), the rapidity y is the same as the pseudorapidity η:

$$y = \frac{E + p_L}{E - p_L} \approx \frac{1 + \cos\theta}{1 - \cos\theta} = -\ln\left(\tanh\frac{\theta}{2}\right) = \eta \tag{3.4}$$

The distributions for method A (green line) and method B (red line) are shown in figure 3.3. In general, all distributions show a similar shape. The differential cross section satisfies

$$\frac{d\sigma}{dy}(-y) = \frac{d\sigma}{dy}(y). \tag{3.5}$$

This symmetry is expected, as there is no reason why there should be a preferred direction of emission in the angle θ. Analysing equation 3.3, the distributions for heavier particles are supposed to be more narrow, whereas lighter particles have a wider 'plateau' around $y = 0$, since the rapidity y is proportional to the inverse mass. This consideration is confirmed in figure 3.3: the gluino yields a more narrow distribution than the squark.[4]

The distributions for the two subtraction methods are very similar for both cases of final

[4]The difference is again even more significant if one compares these distributions to the ones for the SM particles, as they are much lighter and hence have a wider plateau.

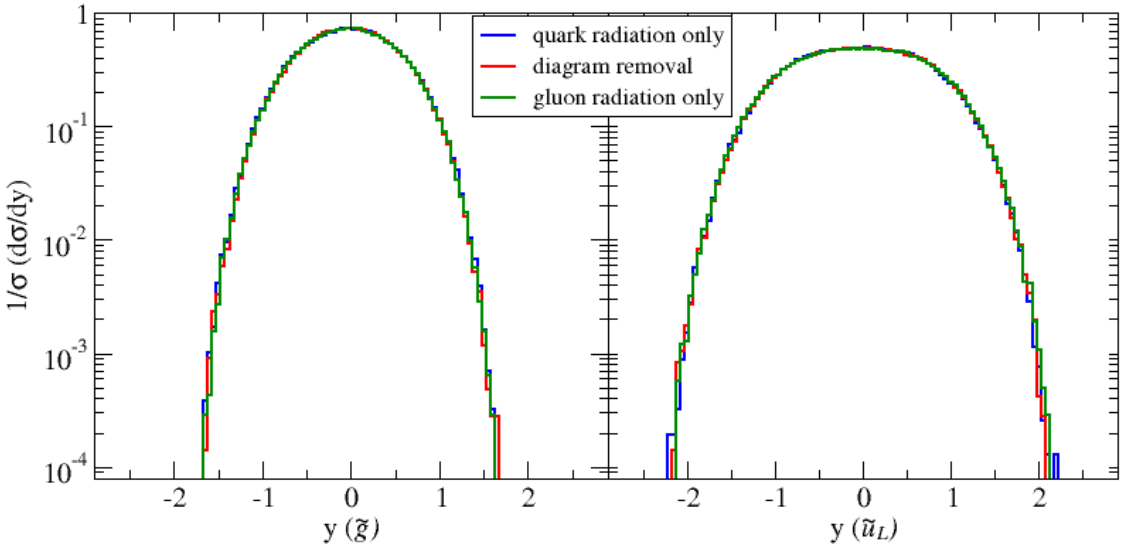

Figure 3.4: **The normalised differential cross section $\frac{d\sigma}{dy}$ of the rapidity of the two final states.** The red and green lines are the same as before. The blue line corresponds to the method where only quarks in the final state are allowed and the diagrams with s-channel gluinos are removed by hand. The shape is basically the same.

states. The shapes agree very well. Small deviations result from statistical fluctuations. As in section 3.2.1, the distributions are normalised to their total cross sections, which differ for both methods as explained previously. To ensure that the methods in these distributions remain consistent, figure 3.4 additionally illustrates the distribution of quark jets. Again, the profiles of the distributions are very similar.

3.3 Numerical subtraction in MadGraph/MadEvent

3.3.1 Distribution in transverse momentum p_T and rapidity y

As discussed in section 2.2.4, the combination of MadGraph/MadEvent and Pythia provides the possibility to exclude specific particles as resonant intermediate states. In order to study this method further, differential cross section depending on the rapidity and the transverse momenta of the final state particles are compared to the two previous ones: gluon radiation and the explicit diagram removal. The results can be seen in figure 3.5 and figure 3.6.

The shape of method C, i. e. using the Excres option in MadGraph/MadEvent, agrees with the other two distributions. The main difference is that, because depending on equation 2.1 more events are rejected with respect to method A and B, the shape

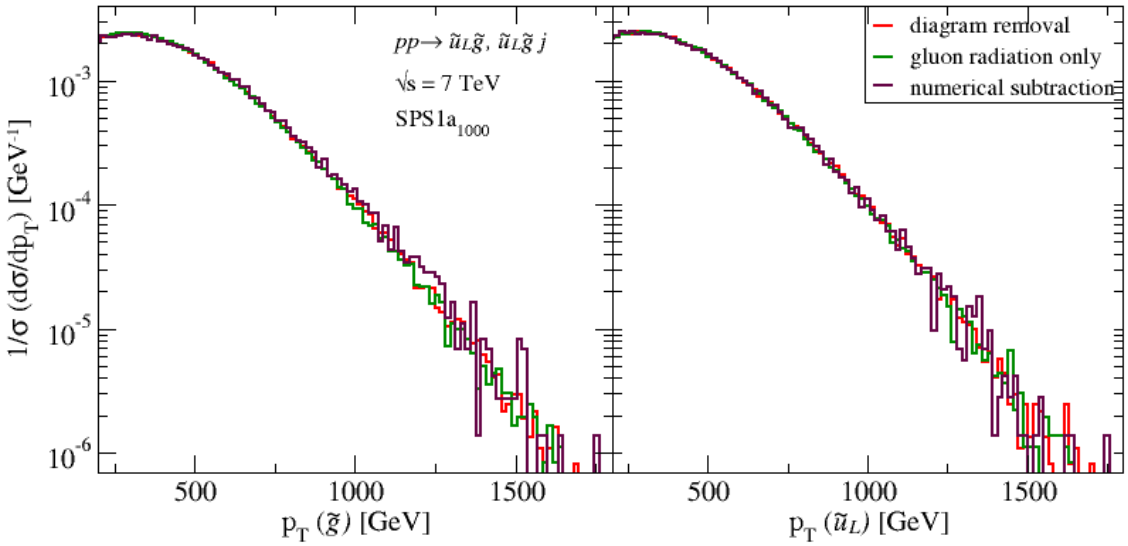

Figure 3.5: **The normalised differential cross section $\frac{d\sigma}{dp_T}$ dependent on the transverse momentum of the two final states.** The green line corresponds to method A, the red one to method B. For the violet distribution, the EXCRES option in MADGRAPH/MADEVENT has been used. In spite of less statistics, it agrees quite well with the other two methods.

shows more statistical fluctuations for the same number of requested events. To improve the appearance of the shape and eliminate the large statistical fluctuations, one therefore has to request more statistics beforehand in method C. The peak of the distribution for the EXCRES method in the gluino rapidity seems to be shifted slightly towards a positive value. It has been confirmed that this is only due to statistics: With more statistics these fluctuations disappear and the distribution is also symmetric to $y = 0$.

3.3.2 Dependence on the width

As explained in section 2.2.4, this way of eliminating the resonant events depends on the width of the on-shell particle, see equation 2.1. To see this explicitly, the dependence of the cross section on this value is studied. Here, the width does not need to be the physical width. It is used only as a regulator.

To see how the cross section qualitatively changes when changing the gluino width, the parameter is varied and to each width the value for the cross section that is given by PYTHIA after showering is assigned. The result can be found in figure 3.7. The dependence of the cross section in the diagram removal method is also plotted for comparison. When removing explicitly potentially on-shell divergent diagrams, there is, as expected, almost no dependence. The slight dependence comes from the fact that there are still diagrams left which involve (in this case) a gluino in the t-channel. These are not on-shell

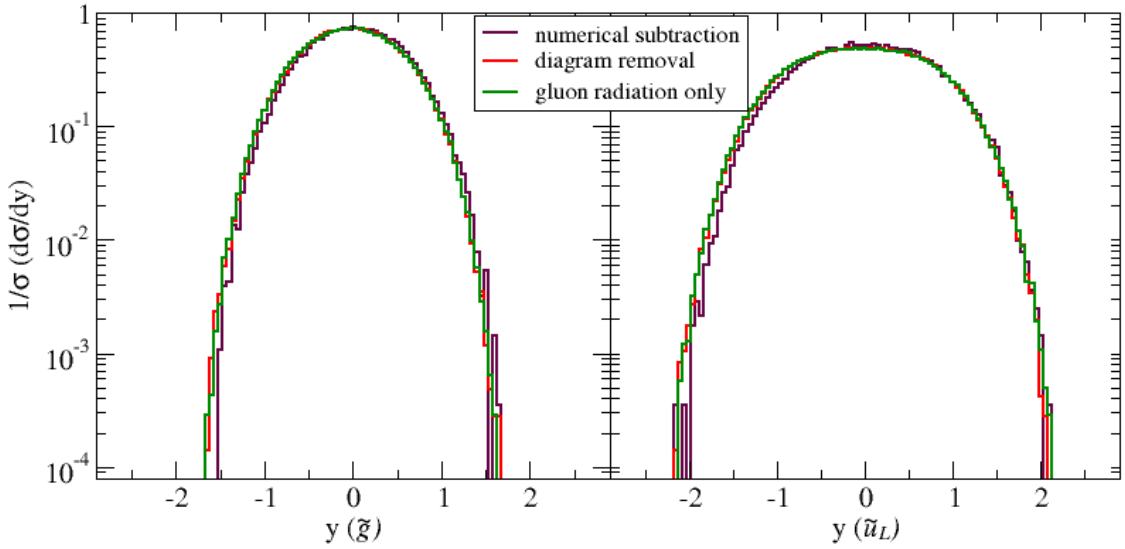

Figure 3.6: **The normalised differential cross section $\frac{d\sigma}{dy}$ depending on the rapidity of the gluino and the squark.** The green line corresponds to method A, the red one to method B and the violet one has been created using the EXCRES option in MADGRAPH/MADEVENT. The three methods agree in the shapes of the distributions. The small deviation for the EXCRES method is due to statistical fluctuations, as many events are lost in this method and therefore the statistics are not as large as for the other two methods.

divergent diagrams and are therefore not removed.

Using the numerical method, there is a strong dependence on the width. The shape nonetheless seems reasonable. If a very large width is used, then according to equation 2.1 almost all potentially resonant events contain on-shell particles, as there is no way for the momentum flow to be outside the region that is defined to be on-shell. Hence, in the limit of very large widths, diagram removal and the numerical subtraction of on-shell divergences is effectively equivalent. In the limit of very small widths, the cross section seems to diverge. This is clear because the width is used as regulator: if the regulator goes to zero, the singular region will be reached. Thus, the cross section diverges.

As there are no errors assigned to the values of the cross section in PYTHIA and these values strongly depend on the specific procedure used in PYTHIA, figure 3.7 only gives a qualitative impression. Physically more meaningful than total cross sections given by PYTHIA are distributions in different kinematic variables.

To that aim, the differential cross section of one final state particle, the squark $\tilde{u}_L$, dependent on the transverse momentum is chosen and plotted for three different widths: $\Gamma_{\tilde{g}} = 10^{-3}$ GeV, 10^{-2} GeV and the physical width $\Gamma_{\tilde{g}}^{phys} = 130.9$ GeV, corresponding to the SPS1a$_{1000}$. The physical width has been calculated by the tool SDECAY [26],

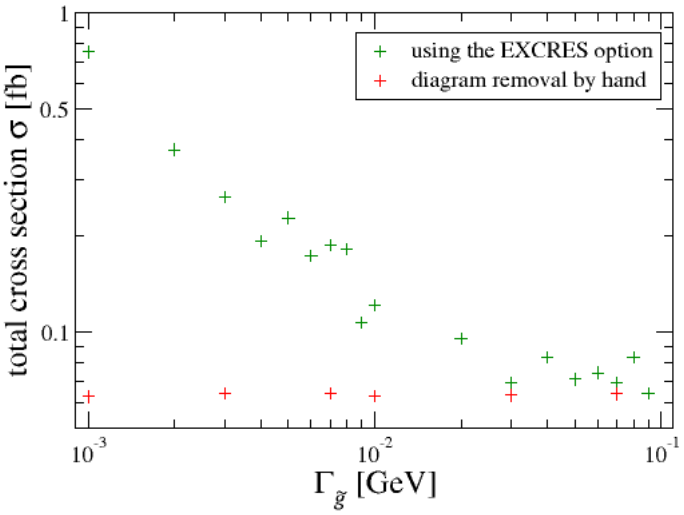

Figure 3.7: **Dependence of the cross section on the width using the Excres option and for comparison in the diagram removal scheme.** The red points correspond to diagram removal, the green ones have been created using the Excres option. Removing the potentially resonant diagrams by hand does not significantly depend on the width as expected. As the cutoff for the Excres option depends on the width, this results also in a quite strong dependence on the width for the cross section.

that calculates all decay widths and branching ratios for supersymmetric particles. The resulting plots can be seen in figure 3.8.

For diagram removal, changing the width does not significantly alter the shape. Considering method C, i. e. the numerical subtraction, there are small changes in the shapes while varying the width. The distribution gets slightly harder, i. e. it is shifted to larger values of the transverse momentum, for larger widths. For smaller widths, this method seems to favour the lower p_T bins, whose events are less likely to fall into the subtracted region of the phase space.

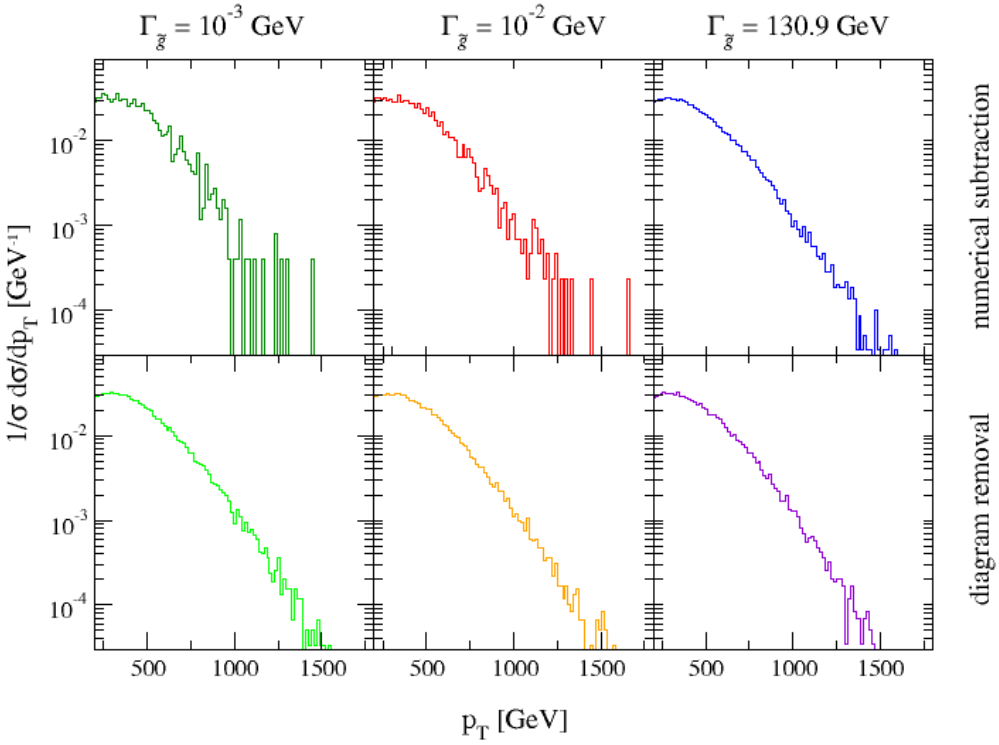

Figure 3.8: **Dependence of the differential cross section on the width, using the Excres option and for comparison in the diagram removal scheme.** The first row corresponds to the EXCRES option, whereas the second row comes from diagram removal. The values for the widths in the three columns are 10^{-3}, 10^{-2} and the physical gluino width 130.9 GeV, respectively. When removing the diagrams by hand, there is no significant dependence on the width. In the EXCRES procedure, one can see a slight dependence on the width as the spectra get slightly harder for larger widths. In the case of a very large width, the shapes for diagram removal and the numerical subtraction of on-shell divergences tend to converge, which is in agreement with figure 3.7.

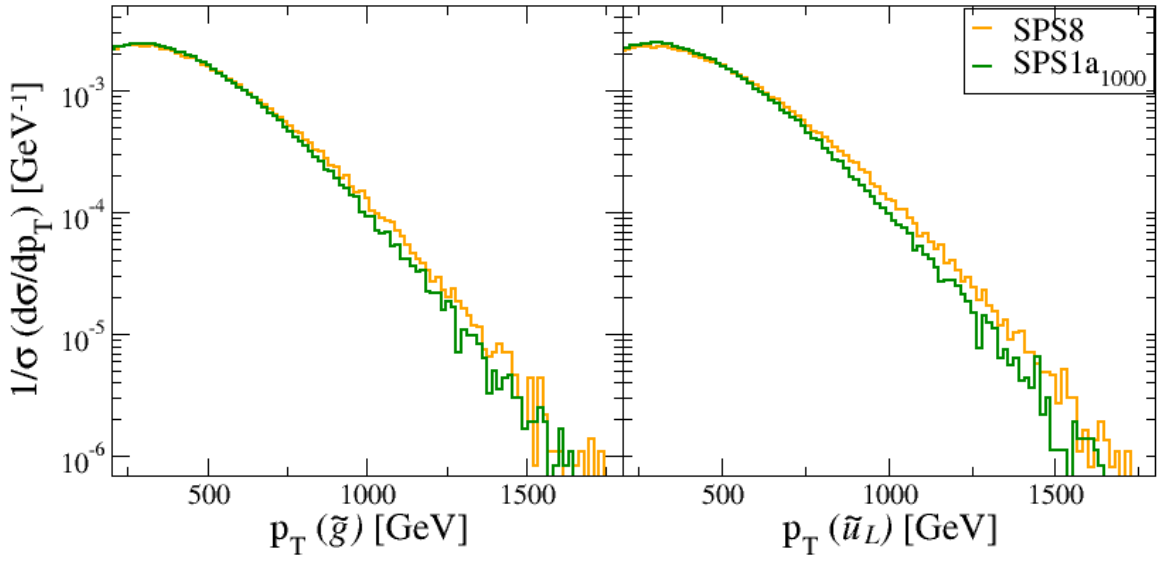

Figure 3.9: **The normalised differential cross section $\frac{d\sigma}{dp_T}$ depending on the transverse momentum of the two final states.** The green line corresponds to the modified SPS1a benchmark point, the yellow line to the SPS8 benchmark point where the mass hierarchy is inverted. In the SPS8, the shape for the gluino is slightly harder compared to the one in the SPS1a_{1000} and even more for the squark. This is due to the set of masses for the heavy coloured particles, which is in this scenario larger than in the SPS1a_{1000}. The gluino mass is only slightly changed to a smaller value in the SPS8, whilst the squark masses in contrast are almost twice as large.

3.4 Different mass hierarchy

As the original benchmark point SPS1a is already ruled out by experiments and currently an inverted mass hierarchy ($m_{\tilde{g}} < m_{\tilde{q}}$) seems to be more likely, the benchmark point SPS8 is considered. The parameters can be found in table 2.2. Again, the dependence of the differential cross sections on the rapidity and the transverse momentum, respectively, are plotted. For simplicity, for both benchmark points the subtraction method A (only gluon radiation) is used. The results are shown in figure 3.9 and figure 3.10.

There are significant differences in the distributions. The p_T distributions in the benchmark scenario SPS8 are slightly shifted to larger transverse momenta. This can be explained by the fact that the heavy particles' masses are significantly larger in this scenario than in the SPS1a_{1000}. The mass of the gluino is slightly smaller in the SPS8, but in contrast the squark masses are almost twice as large.

This mass difference also explains the differences in the shapes of the y distributions. For the gluino, the distributions for the two benchmark points only differ by a small extent. For the squark, however, there is a significant difference. The shape for the SPS8 is

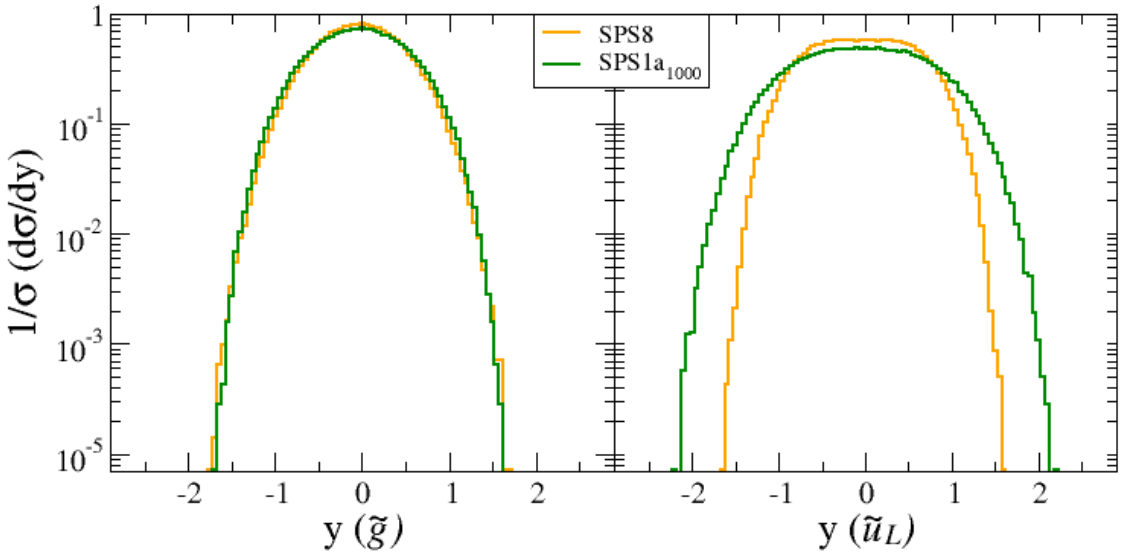

Figure 3.10: **The normalised differential cross section $\frac{d\sigma}{dy}$ depending on the rapidity of the two final states.** The green line represents the modified SPS1a benchmark scenario, the yellow line the SPS8. The spectrum for the gluino is only fractionally more narrow in the SPS8 compared to the SPS1a$_{1000}$. The shape for the final state squark differs significantly in the two scenarios. Due to the almost twice as large masses for the squarks, the form is more narrow.

much more narrow because its mass in this scenario is almost twice as large. For further studies one could compare the different subtraction methods also in this scenario, but in principle, it will be similar to the studies for SPS1a$_{1000}$.

4 Prospino scheme: Comparison of matched samples with the NLO

As the PROSPINO method [8, 9], i. e. the analytical on-shell subtraction, is not implemented yet at leading order in MADGRAPH/MADEVENT, a comparison between the different subtraction methods is not possible in MADGRAPH/MADEVENT yet. But it is part of the NLO package MADGOLEM and therefore analyses can be done at the full NLO but not including parton showers. The studies in section 4.2 and section 4.3 follow closely those in [10].

4.1 Dependence on the width

In the PROSPINO on-shell subtraction, the width of the on-shell particle is used as regulator. For this reason, the dependence of any physical observable on the width is supposed to cancel in the end. To see this, a scan of the cross section in the variable $\alpha_{\text{os}} = \Gamma_{\tilde{g}}/m_{\tilde{g}}$ is done in MADGOLEM. As the subtraction only takes place in the real correction sector, only one subprocess containing potentially on-shell contributions is considered: two gluons scattering into a squark, a gluino and an additional anti-up quark. For comparison, this study is also done for the diagram removal in this subchannel, which is not expected to depend significantly on the width. The resulting plot can be seen in figure 4.1.

The green data points are created using a number of integration points of 10 million, 50 iterations and an accuracy of 10^{-4} to reduce the errors and obtain a very precise result. The diagram removal as reference does not need to be studied in detail here, so to reduce computation time only 10000 points, 50 iterations and an accuracy of 10^{-3} are used. The diagram removal shows no significant dependence on the width. A slight dependence comes from t-channel gluinos, see explanation in 3.7.

In the PROSPINO scheme [8, 9], the cross section starts to rise for very large widths and approaches the rate for diagram removal, whereas for very small ones the errors rise. In between, the cross section is constant while changing α_{os} and thereby the width. In the limit of very small values of α_{os}, the singular region of phase space is reached and therefore the errors by the MC integration get larger. In the limit of very large α_{os}, almost all diagrams involving potentially on-shell intermediate states are removed, i. e. it is effectively the same as diagram removal.

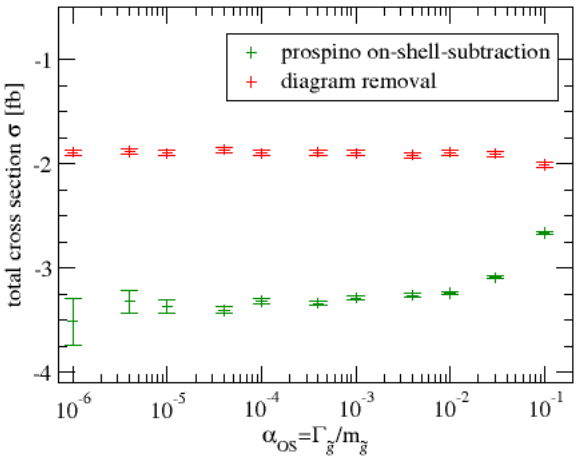

Figure 4.1: **Dependence of the cross section on the gluino width in the Prospino scheme.** Here, only one subprocess, i. e. $gg \to \tilde{g}\tilde{u}_L$ including only additional real emission at NLO, is shown. It is in this case negative which comes from the definition of the counter terms for the divergences. The sum of all NLO corrections is positive as well as the LO. For comparison, the results using diagram removal are shown.

There is a significant difference in the rates for the two methods, i. e. diagram removal and Prospino. In diagram removal, significant contributions are neglected: all diagrams involving a potentially resonant intermediate heavy particle, in this case a gluino, are completely removed, no matter if they are really on-shell or not. In the Prospino scheme, the off-shell contributions are also taken into account and only events in the singular region are subtracted.

4.2 Full NLO versus MLM matching

Experimentally meaningful is the comparison of the full NLO in MadGolem to the matched sample at leading order in MadGraph/MadEvent plus one additional jet. For more precise studies, one could also take into account two additional jets. But in chapter 5 one can see that this can be neglected as a very small correction.

The full NLO matrix elements are generated in MadGolem. For this purpose, the LHC design energy of 14 TeV, a number of integration points of 30000, 15 iterations and an accuracy of 10^{-5} is used. The benchmark scenario SPS8 is chosen, where the squark masses are larger than the gluino mass. The process generation is divided into three subfolders, the leading order (LO), virtual corrections and real corrections. Dimensional

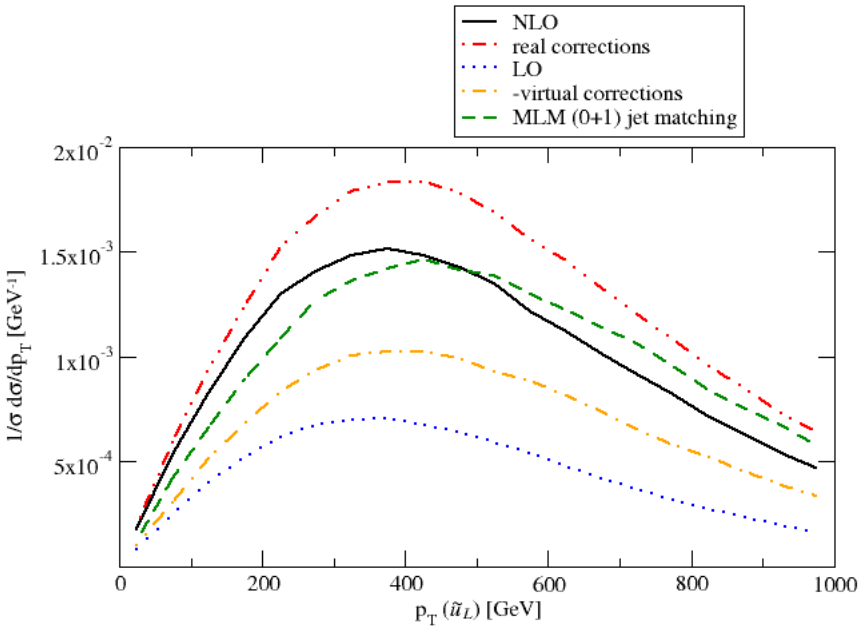

Figure 4.2: p_T **distribution for the squark $\tilde{u}_L$ in NLO (LO, real and virtual corrections) and in comparison with MLM-type matching using the Excres flag in MadGraph/MadEvent.** The NLO has been created in the framework of MadGolem, the MLM-type matching in MadGraph/MadEvent, interfaced with Pythia. For the subtraction of on-shell singularities, the Excres option is used. The green line corresponds to the MLM-type matching. It is harder than the NLO distribution. This makes sense, as there are extra recoil jets in the jet matching that lead to a harder p_T spectrum.

regularisation is used to regularise the ultraviolet and infrared divergences. The resulting UV poles are absorbed in the renomalisation procedure, while for the infrafred a Catani-Seymour subtraction [13] is used. For the latter the subtraction parameter $\alpha = 10^{-3}$ is chosen. This is the reason for the negative virtual corrections. The resulting plot can be seen in figure 4.2.

The green dashed line corresponds to the MLM-type matching. The on-shell singularities in this case are removed with method C, the Excres option. The p_T spectrum for the MLM-type matching is harder than the NLO. This makes sense, as there are additional recoil jets for the jet matching coming from the parton shower. These lead to a recoil of the heavy particles and hence larger values of the transverse momenta.

4.3 NLO Prospino versus NLO diagram removal

From a theoretical point of view, the comparison between diagram removal, which is an approximation for removing on-shell singularities and consequent double counting,

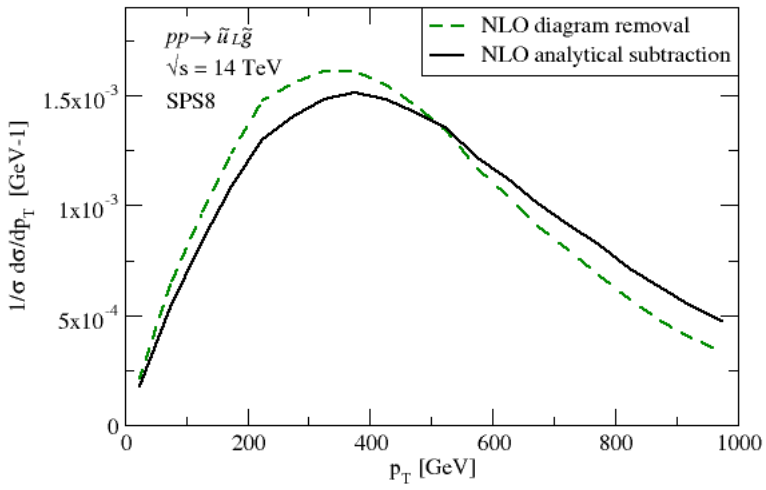

Figure 4.3: Comparison between the diagram removal by hand (green dashed line) and the PROSPINO analytical on-shell subtraction (black full line), both at NLO. The diagram removal gives a softer p_T spectrum.

and the fully analytical subtraction of on-shell parts in the PROSPINO scheme is worth studying. [8,9]. Both p_T distributions are computed at NLO in MADGOLEM. As already pointed out, no showering effects are taken into account. The plots can be found in figure 4.3. The green dashed line corresponds to the NLO with diagram removal, the black line to the NLO with analytical on-shell subtraction.

The p_T spectrum, where the potentially resonant diagrams are removed by hand, is shifted to smaller values of the transverse momentum compared to analytical on-shell subtraction. The difference in this case is significant. If the diagrams that contain potentially on-shell particles are explicitly removed, one neglects contributions that might be important. Not only the part of phase-space, where these diagrams include on-shell particles, is cut off, but the whole diagram is removed. Events coming from those configurations, i. e. including an intermediate off-shell heavy particle (in this case a gluino) outside the singular region, contribute in general to larger transverse momenta. This is why the spectrum is softer for diagram removal, because these events are not included.

In the analytical on-shell subtraction, only the resonant parts are subtracted for each phase space point. There events including intermediate off-shell heavy particles are not neglected and lead therefore to a harder spectrum. Hence the analytical on-shell subtraction is a significant improvement to diagram removal.

5 Multijet matching

So far, only one additional jet has been considered in the studies of this work. In principle, there can be more than just one additional jet. To that purpose, the matching of (0+1) additional jets is compared to the matching of (0+1+2) additional jets. The notation (0+n) means that the computation in leading order (0) plus computations including n additional jets are merged. As in all previous studies, a MLM-type matching implemented in MadGraph/MadEvent is used, as well as the benchmark point SPS1a$_{1000}$. The resulting plots can be found in figure 5.1 and figure 5.2.

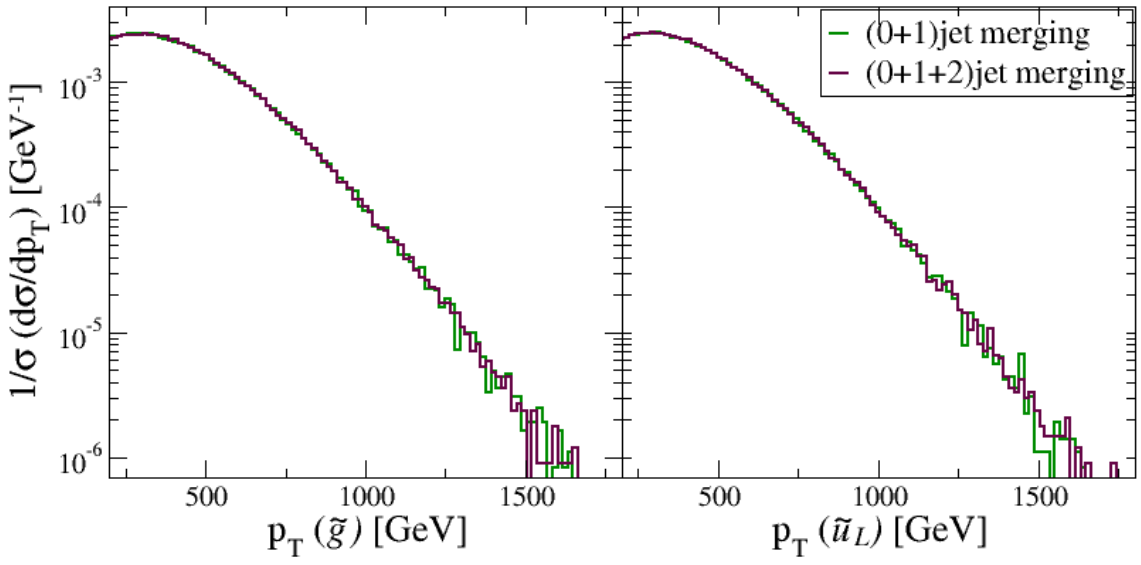

Figure 5.1: **The normalised differential cross section $\frac{d\sigma}{dp_T}$ depending on the transverse momentum of the two heavy final states.** The violet curve includes jet matching with (0+1+2) additional hard jets, whereas the green curve includes only (0+1) additional jet. Both are created using method A, i. e. allowing only for gluons as additional jets to then remove on-shell singularities. The two shapes do not differ significantly.

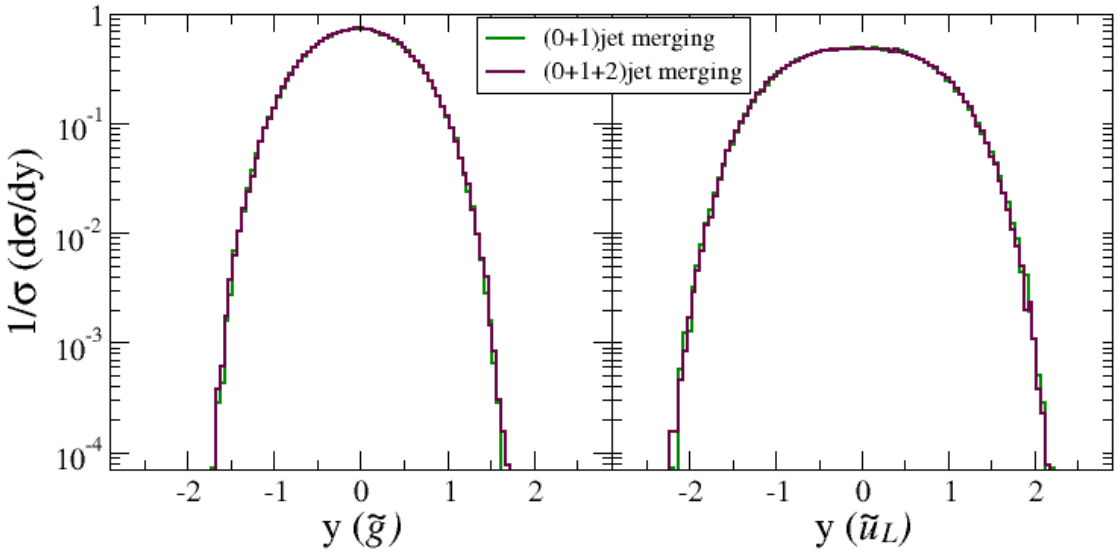

Figure 5.2: **The normalised differential cross section $\frac{d\sigma}{dy}$ in the rapidity of two final state particles.** The green line corresponds to jet matching with (0+1) jet, whereas the violet one also includes a second additional jet. For both curves, only gluon jets are used to avoid on-shell singularities coming from intermediate gluinos. The shapes are very similar, so the influence of the second jet is negligible.

There are no significant differences in the shapes of the two different multiplicity samples. The total cross section values differ slightly, but the distributions for the differential cross sections in the two kinematic variables do not. Thus, it is a reasonable approximation to study distributions including only one additional hard jet.

This agreement between (0+1)-jet matching and (0+1+2)-jet matching shows that the parton shower approximation for the second additional jet is actually quite good. The parton shower describes the emission of jets in all orders in α_s, but only up to a certain transverse momentum. As there is no significant difference in the differential cross section of the two multiplicity samples, the main parts of the events populating the different bins can be assigned to the matching of one additional hard jet and the parton showers. A second jet does not contribute significantly, which means that its main effect is already taken into account by the parton showers. This is further discussed in [30].

6 Conclusions

In this work, different methods to handle on-shell singularities and the related double counting problem were studied. To that endeavour, kinematic distributions of the differential cross section for two kinematic variables, the rapidity and the transverse momentum, respectively, were compared.

In summary, allowing only for extra gluon jets and the explicit diagram removal are gauge violating methods but numerically lead to very similar shapes. Using the Excres flag in MadGraph/MadEvent [5] and Pythia [34], i. e. numerically subtract the on-shell divergences, is in general an improvement to the former methods since not the diagrams are removed, but only those events containing an on-shell particle. This method uses a somehow arbitrary phase space cut which acts as a numerical counterterm to subtract the on-shell singularities. Its results dependent on the width of the on-shell particle, which is due to the definition of 'on-shell' in the context of this method. However, the numerical performance is also similar to diagram removal and gluon radiation only.

The most precise method is the fully analytical subtraction of the on-shell singularities in the Prospino scheme [8, 9], which is gauge invariant. It is part of the full NLO computation, implemented in MadGolem. Hence, no parton showers were used in this method. Comparing the full NLO, using the analytical subtraction, to jet matching (here: MLM-type matching) yields two similar kinematic distributions. Jet matching is to a small extent harder because there are extra recoil jets from the parton shower.

At full NLO, diagram removal and analytical on-shell subtraction were also compared. The former yields a softer distribution. This can be assigned to the fact that by removing diagrams, interference terms as well as potentially significant contributions, coming from the those diagrams with off-shell intermediate particles, to the process are neglected. It is therefore much more improved to use the analytical on-shell subtraction, where only those events involving on-shell intermediate particles are subtracted.

In future projects, the Prospino scheme as fully analytical on-shell subtraction should be implemented at LO in MadGraph/MadEvent: then, an analysis including parton showers could be done and therefore also a comparison between the numerical subtraction in MadGraph/MadEvent and the analytical on-shell subtraction in the Prospino scheme. Furthermore, additional distributions, e. g. in the invariant mass, can be studied for a comparison of different subtraction methods.

At the horizon, projects like POWHEG [1, 16, 28] and MC@NLO [17] promise the combination of the full NLO and the parton showers.

References

[1] S. Alioli, P. Nason, C. Oleari, and E. Re, *A general framework for implementing NLO calculations in shower Monte Carlo programs: the POWHEG BOX* (2010). arXiv:1002.2581[hep-ph].

[2] D. S. M. Alves, E. Izaguirre, and J. G. Wacker, *It's On: Early Interpretations of ATLAS Results in Jets and Missing Energy Searches*, Phys.Lett.B **702:64-68,2011**. arXiv:1008.0407v3[hep-ph].

[3] J. Alwall, S. de Visscher, and F. Maltoni, *QCD radiation in the production of heavy colored particles at the LHC*, JHEP **0902:017,2009**. arXiv:0810.5350v1[hep-ph].

[4] J. Alwall, P. Demin, S. de Visscher, R. Frederix, M. Herquet, F. Maltoni, T. Plehn, D. L. Rainwater, and T. Stelzer, *MadGraph/MadEvent v4: The New Web Generation*, JHEP **0709:028,2007**. arXiv:0706.2334.

[5] J. Alwall, M. Herquet, F. Maltoni, O. Mattelaer, and T. Stelzer, *MadGraph 5: Goying Beyond* (2011). arXiv:1106.0522v1[hep-ph].

[6] ATLAS Collaboration, *Search for squarks and gluinos using final states with jets and missing transverse momentum with the ATLAS detector in sqrt(s) = 7 TeV proton-proton collisions* (September 2011). arXiv:1109.6572v1[hep-ex].

[7] B.C. Allanach et al., *The Snowmass Points and Slopes: Benchmarks for SUSY Searches*, The European Physical Journal C - Particles and Fields **C25,2002**, 113–123. arXiv:hep-ph/0202233v1.

[8] W. Beenakker, R. Höpker, M. Spira, and P. M. Zerwas, *Squark and Gluino Production at Hadron Colliders*, Nucl.Phys.B **492,1997**. arXiv:hep-ph/9610490v1.

[9] W. Beenakker, M. Krämer, T. Plehn, M. Spira, and P. M. Zerwas, *Stop Production at Hadron Colliders*, Nucl.Phys. B **515,1998**. arXiv:hep-ph/9710451v1.

[10] T. Binoth, D. Gonçalves Netto, D. Lopez-Val, K. Mawatari, T. Plehn, and I. Wigmore, *Automized Squark-Neutralino Production to Next-to-Leading Order* (2011). arXiv:1108.1250v1[hep-ph].

[11] R. by L.Garren, C.-J. Lin, S. Navas, P. Richardson, T. Sjöstrand, and T. Trippe, *35. Monte Carlo Particle Numbering Scheme*. http://pdg.lbl.gov/2011/mcdata/mc_particle_id_contents.html.

[12] M. Cacciari and G. P. Salam, *Dispelling the N^3 myth for the Kt-jet-finder*, Phys.Lett.B **641:57-61,2006**. arXiv:hep-ph/0512210v2.

[13] S. Catani, S. Dittmaier, M. H. Seymour, and Z. Trocsanyi, *The Dipole Formalism for Next-to-Leading Order QCD Calculations with Massive Partons*, Nucl.Phys.B **627:189-265,2002**. arXiv:hep-ph/0201036.

[14] S. Catani, F. Krauss, R. Kuhn, and B. R. Webber, *QCD Matrix Elements + Parton Showers*, JHEP **0111:063,2001**. arXiv:hep-ph/0109231v1.

[15] CMS Collaboration, *Search for Supersymmetry at the LHC in Events with Jets and Missing Transverse Energy*, Phys. Rev. Lett. **107,2011**, 221804. arXiv:1109.2352v1[hep-ex].

[16] S. Frixione, P. Nason, and C. Oleari, *Matching NLO QCD computations with Parton Shower simulations: the POWHEG method* (2007). arXiv:0709.2092[hep-ph].

[17] S. Frixione and B. R. Webber, *Matching NLO QCD computations and parton shower simulations*, JHEP **0206:029,2002**. arXiv:hep-ph/0204244v2.

[18] K. Garrett and G. Duda, *Dark Matter: A Primer*, Adv.Astron. **968283,2011**. arXiv:1006.2483v2.

[19] T. Han, *Collider Phenomenology: Basic Knowledge and Techniques* (2005). arXiv:hep-ph/0508097v.

[20] M. Lindner, D. Schmidt, and T. Schwetz, *Dark Matter and Neutrino Masses from Global $U(1)_{B-L}$ Symmetry Breaking* (May 2011). arXiv:1105.4626v2[hep-ph].

[21] L. Lönnblad, *Correcting the Colour-Dipole Cascade Model with Fixed Order Matrix Elements*, JHEP **0205:046,2002**. arXiv:hep-ph/0112284v2.

[22] M. L. Mangano, *Merging multijet matrix elements and shower evolution in hadronic collisions*, 2004.

[23] M. L. Mangano, M. Moretti, F. Piccinin, and M. Treccani, *Matching matrix elements and shower evolution for top-quark production in hadronic collisions*, JHEP **0701:013,2007**. arXiv:hep-ph/0611129v1.

[24] S. P. Martin, *A Supersymmetry Primer* (2011). arXiv:hep-ph/9709356v6.

[25] D. E. Morrissey, T. Plehn, and T. M. P. Tait, *Physics searches at the LHC* (2009). arXiv:0912.3259v2.

[26] M. Muhlleitner, A. Djouadi, and Y. Mambrini, *SDECAY: a Fortran code for the decays of the supersymmetric particles in the MSSM*, Comput.Phys.Commun. arXiv:hep-ph/0311167.

[27] National Aeronautics and Space Administration (NASA), *WMAP 5-year results - Content of the Universe*. http://map.gsfc.nasa.gov/news/5yr_release.html.

[28] P. Nason, *A New Method for Combining NLO QCD with Shower Monte Carlo Algorithms*, JHEP **0411:040,2004**. arXiv:hep-ph/0409146v1.

[29] T. Ohl and T. Darmstadt, *feynMF: Drawing Feynman Diagrams with LATEX and METAFONT*, 1995.

[30] T. Plehn, D. Rainwater, and P. Skands, *Squark and Gluino Production with Jets*, Phys.Lett.B **645,2007**, 217–221. arXiv:hep-ph/0510144v2.

[31] T. Plehn, *Lectures on LHC physics* (2011). arXiv:0910.4182v3[hep-ph].

[32] J. Pumplin, D. R. Stump, J. Huston, H. L. Lai, P. Nadolsky, and W. K. Tu, *GRACE: GRaphing, Advanced Computation and Exploration of data.*

[33] J. Pumplin, D. R. Stump, J. Huston, H. L. Lai, P. Nadolsky, and W. K. Tung, *New Generation of Parton Distributions with Uncertainties from Global QCD Analysis*, JHEP **0207:012,2002**.

[34] T. Sjöstrand, S. Mrenna, and P. Skands, *PYTHIA 6.4 Physics and Manual*, JHEP **0605:026,2006**. arXiv:hep-ph/0603175v2.

Acknowledgements

First and foremost, I want to express my most sincere gratitude to my advisors Dorival Gonçalves-Netto and David Lopez-Val for their valuable support, patience and very interesting discussions during the whole course of this work. Furthermore, I would like to thank my supervisor Tilman Plehn, whose door was always open, for making this project possible and the possibility to get an insight into actual research. Last, but not least, I want to thank the whole research group for a great time at the institute and interesting discussions over lunch.

Erklärung

Ich versichere, dass ich diese Arbeit selbstständig verfasst und keine anderen als die angegebenen Quellen und Hilfsmittel benutzt habe.

Heidelberg, den 8. März 2012,

Jennifer Kieselmann